Joint Entropy-Based Morphology Optimization of Soft Strain Sensor Networks for Functional Robustness

Thomas George Thuruthel, Josie Hughes, and Fumiya Iida

***Abstract*—Dense and distributed tactile sensors are critical for robots to achieve human-like manipulation skills. Soft robotic sensors are a potential technological solution to obtain the required high dimensional sensory information unobtrusively. However, the design of this new class of sensors is still based on human intuition or derived from traditional flex sensors. This work is a first step towards automated design of soft sensor morphologies based on optimization of information theory metrics and machine learning. Elementary simulation models are used to develop the optimized sensor morphologies that are more accurate and robust with the same number of sensors. Same configurations are replicated experimentally to validate the feasibility of such an approach for practical applications. Furthermore, we present a novel technique for drift compensation in soft strain sensors that allows us to obtain accurate contact localization. This work is an effort towards transferring the paradigm of *morphological computation* from soft actuator designing to soft sensor designing for high performance, resilient tactile sensory networks.**

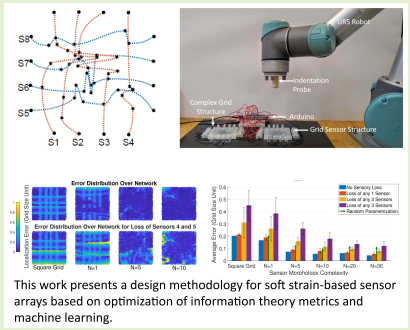

This work presents a design methodology for soft strain-based sensor arrays based on optimization of information theory metrics and machine learning.

***Index Terms*—Soft robotics, tactile sensors, information entropy, optimization methods, machine learning.**

I. Introduction

SOFT strain sensors are becoming increasingly important for soft robotics and wearable electronic devices [1]. They are vital to obtain intrinsic state information like contact, deformation, pressure and stress. Modeling these soft strain sensors is still a major challenge due to their high nonlinearity and time-variant properties [2]. Recent developments in data-driven modeling seems to be a viable solution to circumvent this problem [3]–[6]. However, the morphological design of these sensors have largely been overlooked, mainly because of the lack of analytical models. Soft strain sensors, unlikely traditional sensing technologies, provide immense flexibility in its shape and placement. Coupled with its uniform whole-body receptivity, they could potentially be designed to produce high performance systems. This work investigates an information theoretics-based approach to design better soft strain sensors. Specifically, we look into the design of sensor morphologies that are more robust to damages/loss of data.

Manuscript received April 10, 2020; revised May 11, 2020; accepted May 13, 2020. Date of publication May 18, 2020; date of current version August 14, 2020. This work was supported by the SHERO Project, a Future and Emerging Technologies (FET) Programme of the European Commission under Grant 828818. The associate editor coordinating the review of this article and approving it for publication was Prof. Chang-Hee Won. *(Corresponding author: Thomas George Thuruthel.)*

The authors are with the Bio-Inspired Robotics Lab, Department of Engineering, University of Cambridge, Cambridge CB2 1PZ, U.K. (e-mail: tg444@cam.ac.uk; jaeh2@cam.ac.uk; fi224@cam.ac.uk).

Digital Object Identifier 10.1109/JSEN.2020.2995237

The role of sensor morphology and its adaptation is a well observed phenomenon in nature. Consequently, researchers have tried to apply design principles from nature to robotic sensor systems [7]. The core idea behind these works is that the dynamic and geometric properties of the sensor morphology helps in the pre-processing and structuring of sensory information. Examples of this are the facial whiskers of rodents [8] or the sensilla morphology of the crayfish antennular flagellum [9]. Another interesting implementation of this is how the body morphology can aid external sensor in discerning physical parameters like temperature and stiffness [10]. With the rise in novel materials, technologies and designs in the field of soft robotics, it is crucial that we look into other design methodologies for the development of soft sensors.

The fabrication of soft strain sensors is a rapidly growing field with diverse material-based solutions and manufacturing techniques. They are typically resistance based sensors that respond to geometric changes. Some of the commonly used sensors are based on conductive particles in an elastomeric medium [11], [12] and liquid metal based sensors [13]–[15]. Due to their omni-directional compliance they respond to strain change in all directions. This complicates the modeling process and dilates directional strain sensing properties. However, we gain freedom in the design range and the capability to have the unavoidable rigid wiring far from the sensing region.

Our specific task of interest is in the single-point contact localization using a soft strain sensor based skin [16]. The

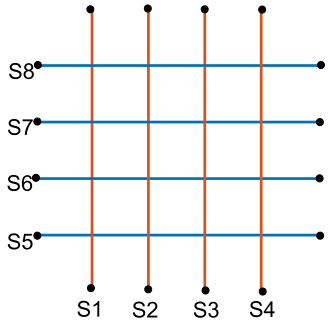

Fig. 1. Typical square grid pattern for soft strain sensors used in contact localization.

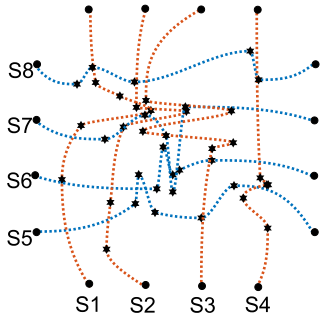

Fig. 2. Parameterization of the sensor morphology. For the above case, each sensor is parameterized by 5 variables in the planar coordinate space (represented by stars). Shape-preserving interpolation is used to obtain the final shape. This is the final sensor morphology used for our experimental validation.

typical design of such sensory networks is in the shape of a square grid (See Figure 1). More complex sensor morphologies has never been investigated due to the lack of accurate analytical models of soft strain sensors. This paper investigates a novel method to design sensor morphologies that perform better in terms of robustness and accuracy. This would allow us to develop sensor networks that maintain functionality during loss of sensory signal or sensor damage. Note that the functionality is not recovered as shown with smart materials [17], [18], but maintained because of redundancy in the system [19]. A similar study was investigated by Culha et. al. to find optimal sensor morphologies for detecting specific kinematic parameters [20], however the sensor morphologies were extracted using exact deformation models.

This work uses metrics from information theory (IT) to evaluate sensor morphologies rapidly with approximate deformation models without the need of accurate sensor models. This is because some of the IT metrics are independent from the actual physics and allows us to easily transfer such models on to the real-world [21]. A purely geometric sensor model with practical constraints is used to develop robust contact localization soft sensor arrays. The optimized networks are first evaluated in simulation for robustness to loss of sensors using machine learning techniques. The derived sensor network is then evaluated experimentally using conductive thermoplastic elastomer-based soft sensors. We present a novel algorithm for sensor drift compensation for quasi-static loading and a perspective on the process of scaling-up tactile sensing ability to larger complex surfaces. Our work is an initial step towards the direction of a scalable approximate methodology for designing better strain-based tactile sensor arrays for soft robotic and wearable applications.

II. Modeling

The main aim of this work is to develop a general framework for evaluation and optimization of sensor morphologies. We are specifically investigating sensor arrays for contact localization. The typical sensor morphology adopted for this purpose is shown in Figure 1, which will be referred to as the square grid from now. Each sensor has a straight morphology in this case. As we are using statistical tools to evaluate a sensor morphology, exact models of the sensors and the enclosing body is not vital. Hence, we can employ simple, static, geometrical models to design our sensor morphology.

A. Morphology Parameterization

To investigate different sensor morphologies, we parameterize each sensor with N variables. The number of sensors in a grid is denoted by $2M$, where M is the number of sensors on each side. For this study we always consider the symmetric grid shape and hence the number of sensors on each side would be same throughout. Each parameter corresponds to a point (with coordinates x, y) in the grid. The starting point and end point of each sensor is always fixed and corresponds to its counterpart in the square grid morphology. The piecewise cubic hermite interpolating polynomial (PCHIP) interpolation is then used to derive the shape of the sensor from the N variables. The MATLAB *fit* function is used for this operation. The PCHIP interpolation function is a shape-preserving interpolation and therefore ensures that the sensor network does not leave the grid. Through this parameterization, the complexity of the sensor morphology can be increased easily by just increasing the value of N. The complete sensor network is hence fully defined by $2 \times MN$ variables (Figure 2).

B. Deformation Model

The deformation model determines the strain values observed in each of the sensor for a given morphology. For simplicity, we study only the static response of the sensors to a single contact. We assume that the strain observed in the sensors is only a function of the shape of the sensor within the deformation area. Any effect of stress concentration due to pre-strain, uneven material distribution and crosstalk is assumed to be absent. We parameterize the deformation area as the polygon formed by a set of points as shown below:

$$\begin{aligned} D_x(i) &= K.cos(2\pi D/i) + Pos_x \\ D_y(i) &= K.sin(2\pi D/i) + Pos_y \quad \forall\, i = 1 \,..\, D \end{aligned} \tag{1}$$

where $[Pos_x, Pos_y]$, is the center of the deformation, K is the size of object that causes the deformation, and D determines the shape of the deformation. A large value of D approximates a circle and a perfect square is defined by a D of 4.

Once the deformation shape and location is defined, the strain values in each sensor can be determined. We will employ a numerical method to obtain the deformation-to-strain values.

The model determines the strain values from the length of the sensor within the deformation area scaled by the inverse of its distance from the center of the deformation (2).

$$s_m = \sum_{p=1}^{P} \Delta d_p / dist_p \quad \forall\ m = 1\ ..\ 2M \tag{2}$$

Here, Δd_p is the length of each numerically quantized segment within the deformation area, P is the number of quantized segments, and $dist_p$ is the distance of each segment from the deformation center.

C. Morphology Assessment and Optimization

Morphology assessment refers to the evaluation of a certain morphology based on a predefined performance metric. It could be based on localization accuracy, robustness to damage, classification accuracy, etc. Ideally, this would involve developing further models to map the raw strain sensor values to meaningful physical variables. However, this is a computationally demanding process and would make it practically impossible to search and optimize through all the design parameters.

One way to speed up the sensor morphology assessment is to use information theoretic measures. We employ entropy, a measure of information content, to guide our sensor morphology optimization. Specifically, we will be using the joint entropy measure of the sensor variables. Increasing the joint entropy would increase the information content in the set of sensors and hence makes the sensory array more robust to the loss of individual sensors. For non-redundant localization tasks (where the sensor distribution is sparse with respect to the contact area), increasing the joint entropy would also results in an average increase in localization accuracy.

The joint entropy of the sensor morphology is estimated by a short, continuous and uniform sampling across the sensor surface. Each sample leads to a change in strain values of certain sensors. Here, we are assuming this strain value is measured using a strain-based soft resistive sensor. Usual soft strain sensors work on changes in resistance induced by strain due to geometric effects, piezoresistive effects, disconnection mechanism, crack propagation and/or tunneling effects [1].

The strain values are then normalized and quantized to the resolution of the measurement device (4096 in our case, as we will be using a 12-bit analog-to-digital converter for our experiments). This would correspond to the resistance values in the sensors. We are using an open source toolbox for measuring the joint entropy [22]. For Q samples from the sensor network of size $2M$, the joint entropy is measured as:

$$\begin{aligned} J.E &= H(S_1, S_2\ \ldots S_{2M}) \\ S_1 &= [s^1, s^2\ \ldots s^Q] \end{aligned} \tag{3}$$

Note that the actual resistance value is not used for measuring the joint entropy values. We assume that the actual resistance values are a monotonic function of the strain values and hence would have similar entropy estimates. Increasing the joint entropy of the set of sensors would increase the robustness of the sensor morphology to loss of sensors and potentially the accuracy of the network. However, there are other practical constraints that must be considered for the network to be effective in real-world scenarios. First, the modeling of an optimized sensor morphology would have to be data-driven. The morphology is too complex to develop analytical models. Hence, there are constraints imposed by a learning system on the morphology of the sensor. Second, fabrication of these sensor networks tend to be more difficult when the sensors crisscross each other.

The nonlinear transfer function used in neural networks and normalization of data imposes smoothness constraints on the data. In other words, if the change in sensor response is not smooth with respect to small changes in location of contact, the training algorithms used in the learning process will be affected. Hence the sharpness of the sensor readings is also added as a constraint for optimization. The initial sampling is continuous for this reason.

$$\begin{aligned} Sharpness(Z) &= \sum_{1}^{2M} \sum_{1}^{P-2} |\Delta^2 S| \\ S &= [S_1, S_2\ \ldots\ S_{2M}] \end{aligned} \tag{4}$$

The amount of crisscrossing among sensors is purely geometric and can be numerically measured. For brevity, we are not including the algorithm. The scalar value which provides a measure of the cumulative area of sensor crossing is denoted as C. Now the objective for our optimization problem would be to increase the joint entropy ($J.E$), while trying to decrease the sharpness (Z) and the sensor crossing area (C). The multi-objective optimization problem can be reformulated as a minimization problem:

$$\begin{aligned} &\min_{z} \quad \alpha \frac{1}{J.E} + \beta Z + \gamma C \\ &z = [(x_1, y_1), (x_2, y_2), \ldots (x_{2MN}, y_{2MN})] \\ &x_{min} < x < x_{max} \\ &y_{min} < y < y_{max} \end{aligned} \tag{5}$$

The boundaries of the sensor network determine the values of $x_{min}, x_{max}, y_{min}, y_{max}$. $\alpha, \beta, and\ \ \gamma$ have to be tuned to get the right trade-off between information content, learnability and ease-of-fabrication. Genetic algorithm is used to find the minima of our objective function (5). For other tasks, appropriate constraints and objectives can be added. Note that the optimized morphology might change with the random initialization of the genetic algorithm and the number of iterations used for optimization.

III. Simulation Results

The main objective of this paper is to design sensor morphologies that are more robust to loss of sensory information. It is expected that a more *complex* sensor morphology would be able to span a larger sensing area while maintaining the constraints imposed on it. The simulation tests are used to verify this. The optimized shapes used for the simulation test are shown in Figure 3.

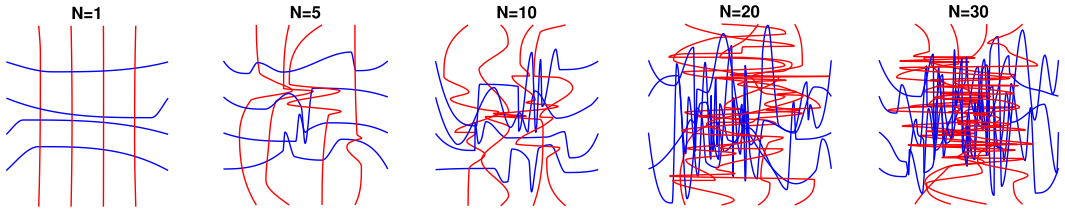

Fig. 3. Optimized shapes of varying complexities.

TABLE I
PARAMETERS FOR THE SIMULATION STUDY

Parameter	Value
Grid Size	1 Unit
Number of Sensors	8
Grid Dimension	4x4 Units
Object Size (K)	0.6 Units
Object Shape Parameter (D)	30
α, β, γ	1, e^{-7},$5e^{-6}$
No. of Samples	1024
Neural Network Size	50

A. Optimization of Sensor Morphology

Once the optimized sensor network is obtained after the optimization process, a larger randomized sampling is performed to test its performance. The results are shown for a grid size (distance between each neighboring sensor) of one unit. The parameters used for the study are shown in table I. A simple single layer neural network is used for learning the mapping from the sensor values to the location of contact, defined by its X and Y coordinates. The Levenberg-Marquardt backpropagation algorithm is used for training with the data divided in the ratio of 70:15:15 for training, testing and validation respectively. To simulate loss of sensory data, we train the neural networks again with lesser number of sensor data. All different combinations of sensory losses are evaluated to find the average performance of the sensor network. For example, for the case of one sensor being damaged, all eight possibilities of sensory loss are considered and evaluated. Using a single network that is robust to loss of input data is still a challenge in machine learning and hence we do attempt to do so. The localization error (root-sum-of-squares) of the neural network is then calculated to evaluate each sensor morphology.

$$LocalizationError = \sqrt{\sum_{i=1}^{1024}(\hat{Y}_i - Y_i^{act})^2}$$
$$\hat{Y}_i = nn(X_i) \quad (6)$$

Here, $\hat{Y}_i$ is the estimated contact location by the neural network (nn) based on the sensor readings X_i. The actual contact location is Y_i^{act}. The average error of the learned model using the optimized sensor network and its robustness to loss of sensory data is shown in Figure 4. For comparison, a randomly generated sensor grid is shown. The results show that the optimization method guarantees an increase in robustness with an increase in sensor complexity. Note that the increase is accuracy is a byproduct of the fact that the localization problem is non-redundant and ill-defined in certain regions

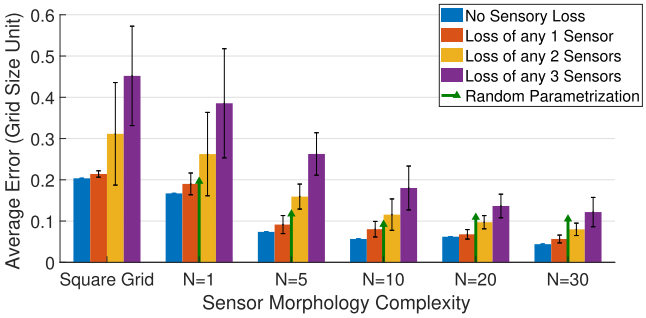

Fig. 4. Performance of the sensor network for different complexity and to the loss of sensory data.

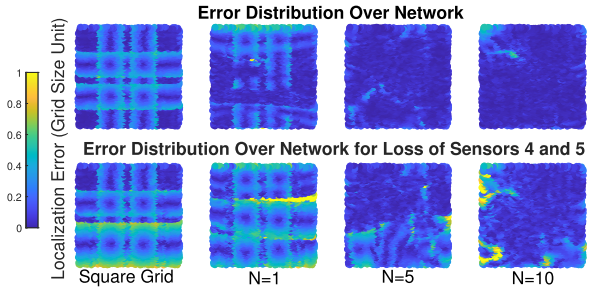

Fig. 5. Localization error distribution for different sensor morphologies. The change in error distribution for an example case is shown below for comparison.

for the square grid. For larger deformations, as shown later, this is no longer the case.

To visualize the dependence between localization error and the contact location, the error distribution across the sensor network is shown in Figure 5. The error heatmap reveals locations where the sensor density is not sufficient or where the sensor readings are not unique. This is clear from the error distribution in the square grid network. The error distribution along the grid for loss of sensory data is also shown for comparison. It can be seen, as expected, that the error distribution becomes more localized and less symmetric with a more complex morphology. Importantly, the new regions of error increase does not correspond with the original error heatmap. Hence they can not only provide higher overall accuracy but can potentially be better at anomaly/damage detection. The detection and localization of sensory damage is easy if the damages are total. Cases where the damage to the sensor affects the performance, but is not disruptive, is more difficult to detect. Here, anomaly detection algorithm using prior learned models are required and morphologies that have unique failure patterns with respect to the baseline performance are better suited for these algorithms.

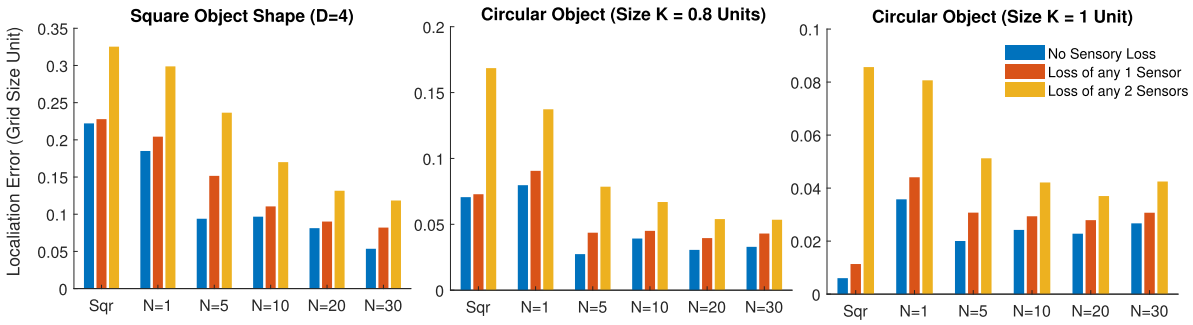

Fig. 6. Sensitivity of the optimized sensor morphologies to the deformation parameters.

B. Sensitivity Analysis

The optimized sensor morphology is obtained for specific deformation models with several additional assumptions. In reality, however there will be considerable differences between the models. It would be difficult and impractical to develop more accurate models to bridge the reality-gap as this weakens the generality of the methodology. The reasoning behind using an information theoretics-based approach is to gain performance improvements without losing generality and by using simple models. The downside being that the derived networks will not be the optimal design for the given task.

To evaluate the dependence of the optimized network on the deformation model we simulate the performance of the optimized morphologies on other deformation parameters. The results are shown in Figure 6. The performance shows similar trends as observed in the original case. As expected, the accuracy of localization increases as the object size increases due to involvement of more sensors. The shape of the object has very little role in the performance. An interesting observation is the drastic accuracy improvement in the performance of the square grid once the object size becomes greater than or equal to the grid size. This is because for this condition, the number of sensors being active becomes greater than three and this helps in removing all the ill-defined inverse mappings where the same sensor readings correspond to different location of contact. Additionally, the linear shape along with the circular deformation provides smooth sensor readings. Non-uniqueness of the sensor-to-location mapping is highly improbably in the complex morphologies due to its asymmetric nature and is therefore not considered as a constraint in the optimization.

C. Perspective: Scaling-up

A potential advantage of the square grid sensor morphology is its ability to scale-up easily. Here, we are referring to ease in terms of modeling difficulty. For an analytical approach, modeling a square grid network does not introduce additional complexities and model complexity would increase linearly with increase in size of the sensor network. The question we are interested is if this property is preserved in a data-driven modeling approach and how we can correspondingly scale-up a complex sensor morphology with practical limits on sampling size.

To study this we obtain samples for learning the localization mapping for sensors of increasing size. We start with the original 4×4 grid and test until a size of 128×128. For each

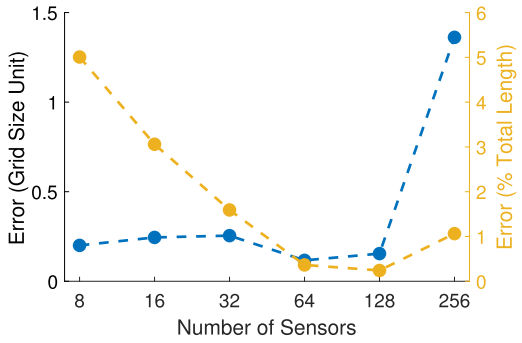

Fig. 7. Localization error with sensor grid dimension for a square grid sensor morphology. The right side shows the average error normalized with the grid dimension. Refer to figure 8 for the error heatmap.

sensor network 4096 samples are obtained and a single layer multilayer perceptron of hidden layer size of 70 is used for learning. The same deformation model and size is used for all the sensor networks. The localization error for different sensor network sizes are shown in Figure 7. It is clear that for the case of 64×64 grid and the 128×128 grid, there has to be loss of information once it enters the network. Nonetheless, the results indicate that the same network size and number of samples is sufficient to attain identical localization accuracy for a square grid sensor morphology. The absolute errors are less the half the grid size unit length up to a sensor grid of size 64×64. The generalization property of neural networks and the symmetry of a square grid makes this feasible. Interestingly, the performance of the sensor grid improves with respect to the sensor network size (localization error goes to 0.24 percent of the network length for the case of 64×64 square grid). This analysis is important because it also indicates that we can potentially reduce the number of wiring to the sensors, based on these simple models and simulation studies. The error distribution along the surface for each sensor network size is shown in Figure 8. It is also interesting that the error distribution is not just dependent on the local morphology of sensor grid (mainly regions where the same sensor readings are obtained at different contact locations), but also reliant on the global morphology (eg. the non repeating error pattern in the 32×32 Grid). Errors due to the local morphology will have repeating patterns due to the symmetry of the design.

Locally, a square grid morphology is not ideal for maximizing entropy. However, global symmetry in a sensor network is beneficial to reduce the effects of the 'curse of dimensionality' in the modeling process. This is not a trivial problem to

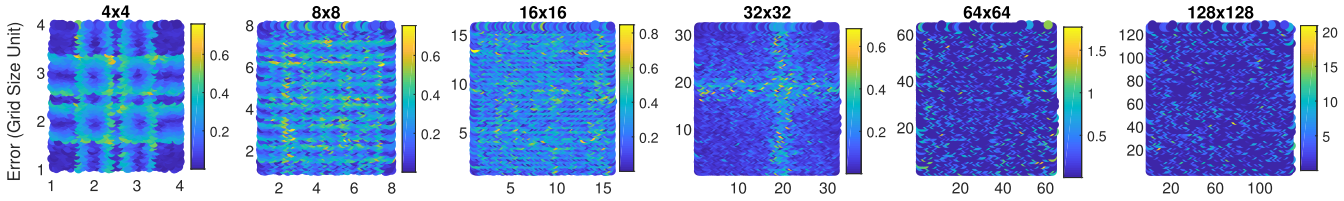

Fig. 8. Error distribution along the surface for increasing sensor dimensionality. Observe that the error distribution is not just dependent on the local morphology (as in the case of the 4 × 4 Square Grid) but also reliant on the global morphology (eg. 32 × 32 Grid).

solve. We are also hampered by the fact that these sensor networks are meant to be embedded in a robotic structure or in wearable devices that have complex geometric shapes. A potential avenue to investigate are fractal structures which are prevalent in nature and in the human nervous system [23]

D. Multi-Contact Localization

The study of multi-contact localization using continuous soft strain sensors have never been investigated before. This is because sensor arrays based on continuum strain sensors are not ideal for multi-contact localization. As a single sensor fibre can be activated in the same manner with contacts at different locations, discrimination of contacts become difficult. This is,of course, one of the drawbacks of using continuous strain sensors for contact localization. For discriminating N contact points without *a priori* knowledge, N independent contact sensors would be required.

Nonetheless, the sensor arrays optimized for single point contact localization can still be tested for multi-point discrimination. As we rely on a learning-based method for localization, the procedure is straightforward. For this study, we investigate the localization accuracy for two-point contact discrimination. Similar to the previous tests, samples are obtained for two independent contacts on the sensor grid. The object size and shape is kept as the default. The samples are increased to 8192 and the network size is increased to 60. The average localization error for both points are shown in Figure 9.

Although, the sensor arrays are not optimized for two simultaneous and independent contacts, it is seen that the complex morphologies still perform better than the square grid morphology. This is not surprising as any break in symmetry and higher area of coverage would most likely improve the discrimination process. For extending the proposed methodology for multi-point optimization, only the sampling process has to modified. Depending on the number of contacts, uniform and unique sampling has be performed for measuring the joint entropy values. Nonetheless, it will be increasingly difficult to perform multi-contact localization with continuous strain sensors. An interesting research question would be analyse how hybrid sensory structures with both discrete and continuous strain sensors can be developed with the help of soft highly conductive material (conductive thread, for example) as bridges.

IV. Materials and Method

A. Conductive Thermoplastic Elastomer

The sensing material used for the development of these soft pads, Conductive Thermoplastic Elastomer (CTPE) is a

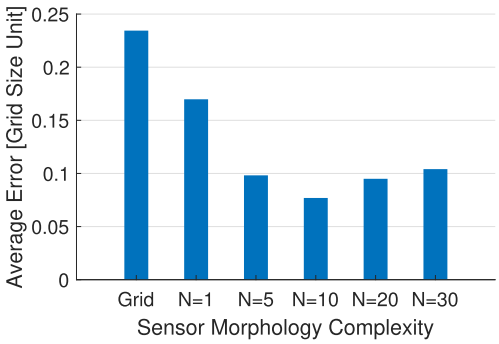

Fig. 9. Two-point contact localization performance.

thermoplastic elastic matrix which is homogeneously mixed with carbon black powder under high pressure and temperature [24]. This process produces an electrically conductive material whose resistance varies with the strain applied [25]. The change in the resistance of materials is caused by the structural deformations of the sensor. CTPE can be extruded into a wide range of shapes or morphologies, including highly elastic fibers typically of 0.3mm diameter, which can undergo strains of above 80% without reaching their tensile limit. This allows the morphology and structure of CTPE sensors to be easily varied. Due to this flexibility, there has been some existing integration into soft robots, and exploration of the optimum sensor morphology for this [26], [27].

B. Fabrication

The soft sensor pads which incorporate the sensor networks has been developed by casting silicone. To accurately fix the sensors in the required position, an inverse mould was made which has small tracks for the sensors to lie in. By exporting the sensor morphologies as images, CAD software was used to create a mould, with these lines extruded slightly above the surface. After 3D printing the moulds EcoFlex 00-20 was cast into the moulds and released after curing. The CTPE sensors were then individually fixed in the tracks using a Dow Corning silicone adhesive to fix them in place and prevent shorts between crossing sensors. Fig. 10 shows the two sensor morphologies which were fabricated.

C. Experimental Setup

To physically test the sensor morphologies, an indentation probe was attached to a UR5 robot arm, with the sensor structures placed in the operation area of the robot. To monitor the changing resistance of the CTPE sensors, they were connected via a matched potential divider to the analogue to digital

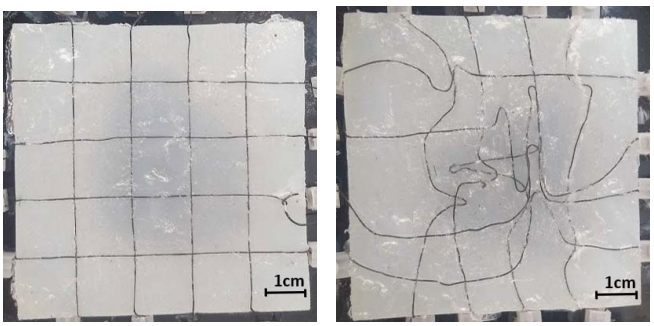

(a) (b)

Fig. 10. Fabricated sensor pads a) Grid based senor morphology, b) Complex sensor morphology.

TABLE II
PARAMETERS OF THE EXPERIMENTAL SETUP

Parameter	Value
Grid Size	11.25 mm
Number of Sensors*	6
Grid Dimension	4x4 Units
Object Size (K)	0.75 mm
Object Shape	Circular Dome
Indentation depth	4mm
No. of Samples	7400
Neural Network Size	50

converters on an Arduino Due. This microcontroller was chosen as it provides the ADC has a 12-bit resolution, allowing small changes in strain to be measured. The control PC was used to read from the Arduino and also control the position of the UR5 robot arm. Fig. 11 shows the experimental setup and a block diagram of the system. The experimental setup is designed to emulate the simulation model. The experimental parameters are shown in Table II. Experimentally, reducing the probe size led to non-repeatable behaviors or damages in the strain sensors, possibly because of high stress concentration. From the simulations, it was clear that increasing the probe size essentially neutralizes the effect of the optimization as more sensors become active. So, we have conducted our experiments only for a single probe size.

V. EXPERIMENTAL RESULTS

The validation of the proposed methodology is done by experimentally comparing the performance of the square grid and the optimized sensor morphology with a N value of 5 (Fig. 10). The sensor morphologies are evaluated by measuring the localization accuracy of the network and its robustness to loss of sensory information. The experimental procedure was designed to closely match the simulation procedure for comparison. The localization models are trained using the parameters shown in Table II. During, the complete sampling process some of the sensors got damaged internally. Therefore, the results are obtained after removing two sensor readings from each of the sensor networks (S1 and S2). As the simulation framework was built on a static model between deformation and strain values, we try to emulate the same on the real sensors. To do so we introduce a novel method for compensation of the time dependent drift based on the uniqueness of the typical drift cycle [28].

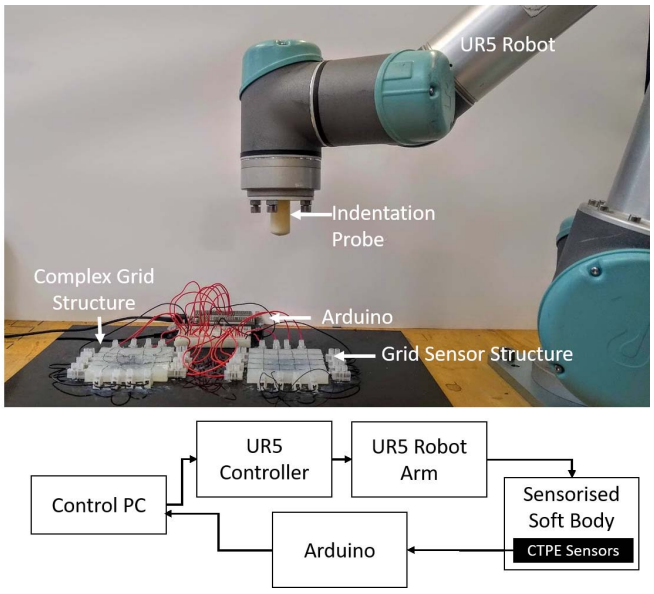

Fig. 11. Experimental setup and block diagram.

A. Drift Compensation

The actual response of a single CTPE sensor to a cycling loading and the actual values during indentation is shown in Figure 12. Due to the drift in the sensor, the absolute values of the sensor resistance do not correspond to the actual strain values. There are few works on dynamic drift compensation [3], [29]. However, here we propose a simpler method for static drift compensation. The proposed learning-based method can work even for high hysteresis sensors. In fact, our sensors are affected by a combination of drift, hysteresis and other nonlinear effects. The method relies on the fact that the time period of the indentation cycle is constant.

First, the sensor values are filtered with a method called total variation denoising. This allows us to reduce noise without smoothing away edges. The drift compensation method relies on the fact that for a fixed period loading cycle, the sensor readings cycle would correspond to the actual strain induced during the process. Hence, given the strain state of the material can be inferred from a rough estimate of the sensor resistance cycle. This information is provided to the neural network as the inputs $[x_{i-1}, x_i, x_{i+1}]$. Where, x_{i-1} is the sensor resistance before indentation, x_i is the sensor resistance during indentation and x_{i+1} is the sensor value during indentation. An example is shown in Figure 12. The localization model, hence is slightly different from the simulated one with the input size being increased by a factor of three.

Due to the presence of drift and our model-free technique for drift compensation, we cannot estimate the true state of sensor strain during the sampling process. Hence, we cannot estimate the joint entropy measure and make a direct comparison with the simulation result. We can still compare ideal period in each sensor in the simulation and the experiment as shown in Table III. For the simulation, this is simply calculated by the average percentage of time a sensor is inactive. As expected, in the complex morphology, the sensors are active more time on average than the grid morphology. For the experimental setup, sensor activation is recorded if the change

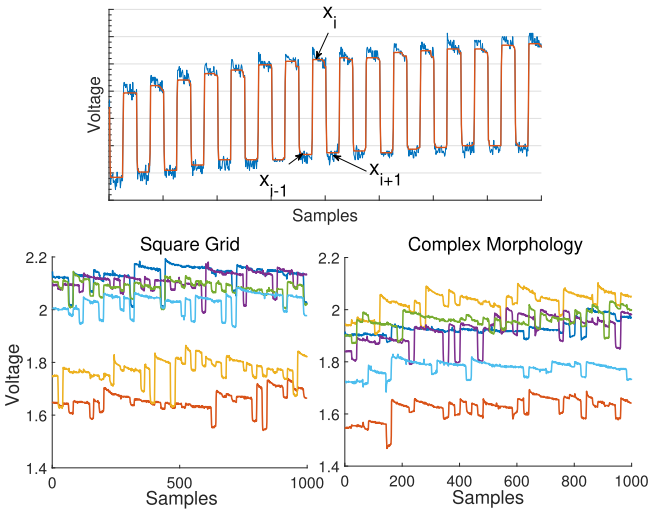

Fig. 12. Above: Typical drift observed in the soft strain sensor and the key variables used in our drift compensation technique. The red plot shows the filtered sensor signal. Below: Raw sensor values used for contact localization.

TABLE III
AVERAGE SENSOR IDLE STAGE: SIMULATION VS EXPERIMENT

Morphology	Simulation	Experiment
Grid	70%	78%
N=5	57%	77%

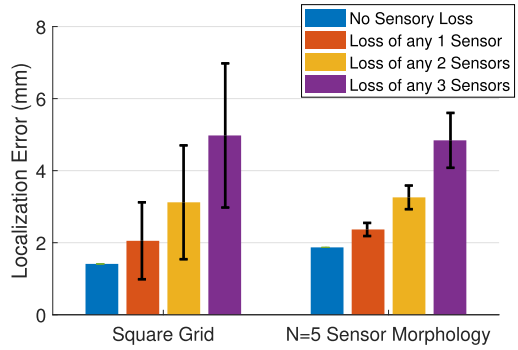

Fig. 13. Localization accuracy of the square grid and the complex sensor morphology. The variance in performance to loss of sensory information is shown using standard deviation bars.

in resistance for each sample is higher than two percentage of the total variation in the resistance obtained across all the observations. The grid morphology performs within reasonable similarity to the simulation as the sensor activation should be dependent only on the geometry of deformation and not on the physical properties of the material. However, for the complex morphology, the average activation is similarly low. This could be because some of the sensors have much reduced sensitivity and possible manufacturing defects.

B. Accuracy and Robustness

The localization accuracy and the robustness of the sensor networks to loss of sensory data is shown in Figure 13. The performance of both the sensor networks are similar with respect to average localization accuracy. The square grid was slightly more accurate (1.7 mm) when compared

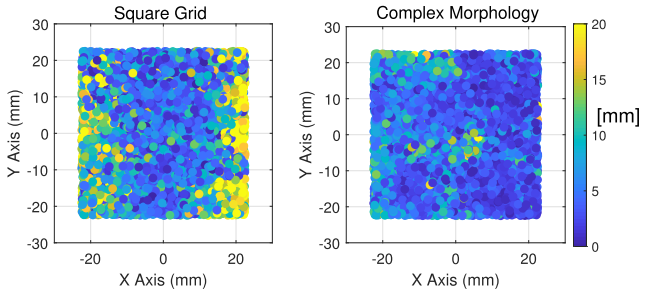

Fig. 14. Localization error along the surface for the removal of three sensors from the same location.

to the complex morphology (2.1mm), when all the sensor data was used for localization. Similar performance trends were observed in simulations when the object deformations had a large area. Indeed, it was observed that due to the high compliance of the enclosing medium, the deformation propagated much farther than the probe size. This also leads to a remarkable robustness of both the network to sensory loss. Both sensor morphologies maintain an average accuracy of 5mm even when only three sensors are active.

The complex morphology is however better suited for high fidelity sensing as it can provide higher error tolerances as shown by the standard deviations in Figure 13. This would ensure consistent performances, irrespective of which sensor is damaged. The performance of the square grid, on the other hand, is highly dependent on this. For instance the maximum error for loss of a single sensor was 4.2 mm for the square grid while the complex morphology had a maximum error of 2.5 mm. Similarly for the loss of two and three sensors the square grid had a maximum error of 6.3mm and 8.2 mm while the complex morphology only went up to 3.9mm and 6.7 mm, respectively.

The error distribution in the complex morphology is shown in Figure 14 for the case of three sensors (S6,S7,S8) removed. The error distribution does not exactly mimic the simulation results. Yet, there are typical high error regions along the edges. Note that it is more difficult to fabricate the complex sensor network than the square grid sensor network. As the sensor threads are placed by hand, localized stretching and compression of the sensor occurs, which affects the signal quality drastically. For the square grid, uniform pre-strain could be achieved easily because of its geometry. With better manufacturing techniques, we expect the complex morphology to perform even better in terms of accuracy and robustness.

To analyze the sensitivity of the prototypes to other probing conditions, tests where also performed with a smaller probe size (half of the default size), similar to the one shown in figure 6. Large probe sizes are not of interest as an optimized sensor network would ideally use the minimum number of sensors and hence the maximum grid size. The tests were performed with all the sensors active, as compared to the previous tests. Both the sensor arrays performed poorly for this case with the complex morphology having an average accuracy of 6.28 mm and the square grid having an accuracy of 6.82 mm. Note that this is with all eights sensors active. We speculate that this is because of large concentrated strains that

the strain sensors experienced with the smaller probe. This lead to large spikes in the sensor values and permanent damages to the sensor itself.

VI. Discussions and Conclusion

The main aim of the paper is to show that just by optimizing the shape of each strain sensor fiber we can achieve better performance without additional sensors or circuitry. We demonstrate a way to achieve this without an actual model of the strain sensor, but with a purely geometrical model and information theory metrics. Such an approach can be easily adopted to different tasks and structures and would be less susceptible to modeling differences. This paper demonstrates how such a method can be used to develop sensor networks that are robust to damages. We are able to achieve this performance improvement solely by the morphology of the sensors, which is unprecedented in the literature. We incur no additional electronics or processing costs. Further, with the use of Information Theory we can rely on very simple geometric models to develop our sensor morphologies. The models are developed without any knowledge about the physical sensor, physical properties of the sensor matrix, the data processing mechanism and accurate deformation values. Extending the work to shape recognition or contact force prediction is also possible with appropriate deformation models and entropy-based metrics. Moreover, we have proposed a novel static drift compensation technique for soft strain sensors(section V A) and perspectives on how such learning-based approaches scale with increasing sensors (section III C). Our current work is limited to static tasks. Considerable improvements can be attained by characterizing the information content from the real soft sensors and their dependence on the deformation parameters. Noise in the signals and the characteristic drift are the main challenges to be overcome to do such studies.

One of the main disadvantages of the complex morphology was the fabrication process. Our current sensor array are made by manually placing sensor threads into cavities in embedding matrix. As the sensor morphology becomes more complex, the fabrication of the sensors become more difficult and introduces undesired pre-strain in the material. However, with the development of new fabrication techniques and materials for 3D printing soft strain sensors [30], [31], this problem can be easily addressed. An alternate approach would be to cast sensor grid using inverse molds. However, additional care has to be taken to ensure uniform distribution and response of the sensor material.

A fascinating result from the experiments is that the observed accuracy of the square grid structure (around 4.5 percent of the network length) was slightly better than the predicted accuracy of the simulated model (around 5 percent of the body length), even though the real-world scenario is noisy and nonuniform. We hypothesize that these minute variations and non-uniformity, either to the material properties or the fabrication technique actually helps in improving accuracy for the square grid. Theoretically, the accuracy of the square grid is limited for an object size of less than 2 times the grid size because of the non-uniqueness of the sensors to contact locations, as observed through our simulation results. This will be reflected in their entropy measures too. The non-uniformity along the sensor network, therefore, helps in resolving this uniqueness issue. Ironically, with consistent material properties and manufacturing techniques we might see a decline in the performance of the square grid sensor morphologies.

Soft strain sensors are highly susceptible to damage. This can be addressed in multiple ways; by smart materials [32], [33], exploiting redundant multi-modal information [3], or finally by smart structures as shown in this paper. Moreover, the effort in wiring and processing the sensor reading with low latency imposes limits on the number of sensors we can deploy in our robotic structures. Hence, an alternative would be the use of optimized sensor morphologies that can provide the same performance with better robustness to loss of sensory data.

A straightforward extension of this work is to extend the design of sensor morphologies for actuated systems. Here, the geometrical effects due to motions of the body and contact with the environment has to be considered. The fundamental difference between deformation induced by intrinsic motion and external environment is the new information provided by the control signals to the actuators. The same methodology can be easily extended to detect multiple contacts with a modified sampling strategy for entropy measurement. Our simulations results show that even the sensor arrays optimized for single-point contact works better for multi-point contact. This is intuitive because by optimizing the joint-entropy for single-point localization, we are increasing the redundancy in the system, which would most likely (not necessarily) lead to better multi-point discrimination. Another possible topic to investigate is the optimization of the three dimensional structure of soft sensors and superficial damage detection using the optimized sensor networks.

Appendix

The complete dataset of the simulations and experiments along with the code can be found here: https://github.com/tomraven1/sensor_morphology

Acknowledgment

The authors would like to thank Frank Clemens (EMPA) for providing assistance and for providing the sensor materials.

References

[1] M. Amjadi, K.-U. Kyung, I. Park, and M. Sitti, "Stretchable, skin-mountable, and wearable strain sensors and their potential applications: A review," *Adv. Funct. Mater.*, vol. 26, no. 11, pp. 1678–1698, Mar. 2016.

[2] H. Wang, M. Totaro, and L. Beccai, "Toward perceptive soft robots: Progress and challenges," *Adv. Sci.*, vol. 5, no. 9, Sep. 2018, Art. no. 1800541.

[3] T. G. Thuruthel, B. Shih, C. Laschi, and M. T. Tolley, "Soft robot perception using embedded soft sensors and recurrent neural networks," *Sci. Robot.*, vol. 4, no. 26, Jan. 2019, Art. no. eaav1488.

[4] D. Kim, J. Kwon, S. Han, Y.-L. Park, and S. Jo, "Deep full-body motion network for a soft wearable motion sensing suit," *IEEE/ASME Trans. Mechatronics*, vol. 24, no. 1, pp. 56–66, Feb. 2019.

[5] I. M. Van Meerbeek, C. M. De Sa, and R. F. Shepherd, "Soft optoelectronic sensory foams with proprioception," *Sci. Robot.*, vol. 3, no. 24, Nov. 2018, Art. no. eaau2489.

[6] L. Scimeca, J. Hughes, P. Maiolino, and F. Iida, "Model-free soft-structure reconstruction for proprioception using tactile arrays," *IEEE Robot. Autom. Lett.*, vol. 4, no. 3, pp. 2479–2484, Jul. 2019.

[7] F. Iida and S. G. Nurzaman, "Adaptation of sensor morphology: An integrative view of perception from biologically inspired robotics perspective," *Interface Focus*, vol. 6, no. 4, Aug. 2016, Art. no. 20160016.

[8] M. J. Pearson, B. Mitchinson, J. C. Sullivan, A. G. Pipe, and T. J. Prescott, "Biomimetic vibrissal sensing for robots," *Phil. Trans. Roy. Soc. B, Biol. Sci.*, vol. 366, no. 1581, pp. 3085–3096, Nov. 2011.

[9] S. Pravin, D. Mellon, E. J. Berger, and M. A. Reidenbach, "Effects of sensilla morphology on mechanosensory sensitivity in the crayfish," *Bioinspiration Biomimetics*, vol. 10, no. 3, Apr. 2015, Art. no. 036006.

[10] S. G. Nurzaman, U. Culha, L. Brodbeck, L. Wang, and F. Iida, "Active sensing system with *in situ* adjustable sensor morphology," *PLoS ONE*, vol. 8, no. 12, Dec. 2013, Art. no. e84090.

[11] T. Yamada *et al.*, "A stretchable carbon nanotube strain sensor for human-motion detection," *Nature Nanotechnol.*, vol. 6, no. 5, p. 296, 2011.

[12] M. Amjadi, A. Pichitpajongkit, S. Lee, S. Ryu, and I. Park, "Highly stretchable and sensitive strain sensor based on silver nanowire–elastomer nanocomposite," *ACS Nano*, vol. 8, no. 5, pp. 5154–5163, May 2014.

[13] Y.-L. Park, B.-R. Chen, and R. J. Wood, "Design and fabrication of soft artificial skin using embedded microchannels and liquid conductors," *IEEE Sensors J.*, vol. 12, no. 8, pp. 2711–2718, Aug. 2012.

[14] J.-B. Chossat, Y.-L. Park, R. J. Wood, and V. Duchaine, "A soft strain sensor based on ionic and metal liquids," *IEEE Sensors J.*, vol. 13, no. 9, pp. 3405–3414, Sep. 2013.

[15] D. M. Vogt, Y.-L. Park, and R. J. Wood, "Design and characterization of a soft multi-axis force sensor using embedded microfluidic channels," *IEEE Sensors J.*, vol. 13, no. 10, pp. 4056–4064, Oct. 2013.

[16] S. Sundaram, P. Kellnhofer, Y. Li, J.-Y. Zhu, A. Torralba, and W. Matusik, "Learning the signatures of the human grasp using a scalable tactile glove," *Nature*, vol. 569, no. 7758, pp. 698–702, 2019.

[17] E. J. Markvicka, M. D. Bartlett, X. Huang, and C. Majidi, "An autonomously electrically self-healing liquid metal–elastomer composite for robust soft-matter robotics and electronics," *Nature Mater.*, vol. 17, no. 7, p. 618, 2018.

[18] S. Terryn, J. Brancart, D. Lefeber, G. Van Assche, and B. Vanderborght, "Self-healing soft pneumatic robots," *Sci. Robot.*, vol. 2, no. 9, Aug. 2017, Art. no. eaan4268.

[19] M. L. Visinsky, J. R. Cavallaro, and I. D. Walker, "Robot fault detection and fault tolerance: A survey," *Rel. Eng. Syst. Saf.*, vol. 46, no. 2, pp. 139–158, 1994.

[20] U. Culha, S. Nurzaman, F. Clemens, and F. Iida, "SVAS3: Strain vector aided sensorization of soft structures," *Sensors*, vol. 14, no. 7, pp. 12748–12770, Jul. 2014.

[21] A. Krause, A. Singh, and C. Guestrin, "Near-optimal sensor placements in Gaussian processes: Theory, efficient algorithms and empirical studies," *J. Mach. Learn. Res.*, vol. 9, no. 2, pp. 235–284, 2008.

[22] *MIToolbox*. Accessed: Aug. 13, 2019. [Online]. Available: https://github.com/Craigacp/MIToolbox

[23] G. Werner, "Fractals in the nervous system: Conceptual implications for theoretical neuroscience," *Frontiers Physiol.*, vol. 1, p. 15, Jul. 2010.

[24] F. J. Clemens *et al.*, "Development of piezoresistive fiber sensors, based on carbon black filled thermoplastic elastomer compounds, for textile application," *Adv. Sci. Technol.*, vol. 80, pp. 7–13, Sep. 2012.

[25] C. Mattmann, F. Clemens, and G. Tröster, "Sensor for measuring strain in textile," *Sensors*, vol. 8, no. 6, pp. 3719–3732, Jun. 2008.

[26] J. Hughes and F. Iida, "Localized differential sensing of soft deformable surfaces," in *Proc. IEEE Int. Conf. Robot. Autom. (ICRA)*, May 2017, pp. 4959–4964.

[27] J. Hughes and F. Iida, "Tactile sensing applied to the universal gripper using conductive thermoplastic elastomer," *Soft Robot.*, vol. 5, no. 5, pp. 512–526, Oct. 2018.

[28] P. Kelly, "Solid mechanics lecture notes," Dept. Eng. Sci., Univ. Auckland, Auckland, New Zealand, Tech. Rep., 2012.

[29] I. M. Van Meerbeek, J. A. Barreiros, R. F. Shepherd, and C. M. De Sa, "Addressing sensor drift in a proprioceptive optical foam system," *Proc. SPIE*, vol. 10970, Mar. 2019, Art. no. 109700F.

[30] B. Shih *et al.*, "Design considerations for 3D printed, soft, multimaterial resistive sensors for soft robotics," *Frontiers Robot. AI*, vol. 6, p. 30, Apr. 2019.

[31] J. T. Muth *et al.*, "Embedded 3D printing of strain sensors within highly stretchable elastomers," *Adv. Mater.*, vol. 26, no. 36, pp. 6307–6312, Sep. 2014.

[32] Y.-J. Liu, W.-T. Cao, M.-G. Ma, and P. Wan, "Ultrasensitive wearable soft strain sensors of conductive, self-healing, and elastic hydrogels with synergistic 'soft and hard' hybrid networks," *ACS Appl. Mater. Interfaces*, vol. 9, no. 30, pp. 25559–25570, 2017.

[33] M. D. Bartlett, M. D. Dickey, and C. Majidi, "Self-healing materials for soft-matter machines and electronics," *NPG Asia Mater.*, vol. 11, no. 1, p. 21, Dec. 2019.